NANO LETTERS

pubs.acs.org/NanoLett Letter

Ligand-Dependent Coalescence Behaviors of Gold Nanoparticles Studied by Multichamber Graphene Liquid Cell Transmission Electron Microscopy

Yuna Bae, Kitaek Lim, Seulwoo Kim, Dohun Kang, Byung Hyo Kim, Joodeok Kim, Sungsu Kang, Sungho Jeon, JunBeom Cho, Won Bo Lee,* Won Chul Lee,* and Jungwon Park*

Cite This: https://dx.doi.org/10.1021/acs.nanolett.0c03517

Read Online

ACCESS | Metrics & More | Article Recommendations | Supporting Information

ABSTRACT: The formation mechanism of colloidal nanoparticles is complex because significant nonclassical pathways coexist with the conventional nucleation and growth processes. Particularly, the coalescence of the growing clusters determines the final morphology and crystallinity of the synthesized nanoparticles. However, the experimental investigation of the coalescence mechanism is a challenge because the process is highly kinetic and correlates with surface ligands that dynamically modify the surface energy and the interparticle interactions of nanoparticles. Here, we employ quantitative *in situ* TEM with multichamber graphene liquid cell to observe the coalescence processes occurring in the synthesis of gold nanoparticles in different ligand systems, thus affording us an insight into their ligand-dependent coalescence kinetics. The analyses of numerous liquid-phase TEM trajectories of the coalescence and MD simulations of the ligand shells demonstrate that enhanced ligand mobility, employing a heterogeneous ligand mixture, results in the rapid nanoparticle pairing approach and a fast post-merging structural relaxation.

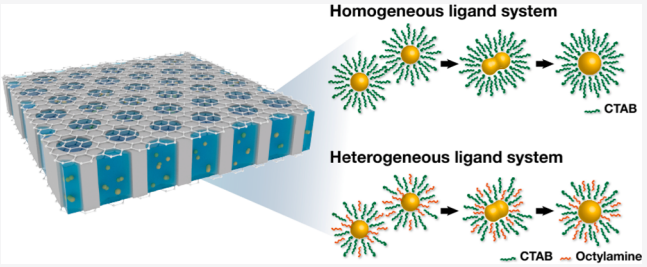

KEYWORDS: *quantitative liquid-phase TEM, in situ TEM, coalescence, ligand-dependency, nanoparticles*

Downloaded via SEOUL NATL UNIV on November 16, 2020 at 03:29:31 (UTC).
See https://pubs.acs.org/sharingguidelines for options on how to legitimately share published articles.

The chemical, catalytic, and optical properties of nanoparticles originate from their structures. Moreover, the morphology and crystallinity of nanoparticles are determined during their growth in colloidal synthesis. Nanoparticles with an anisotropic morphology, a polycrystalline structure, and defects are frequently formed by coalescence, known as a nonclassical pathway for nanoparticle growth, which results in unique functionalities. For example, nanoparticles with high grain boundary densities or multifold twin structures have been synthesized as materials with enhanced catalytic activity due to the modified active sites on their surfaces or interfaces.[1] Additionally, high-branched nanoparticles, which exhibit unique spectroscopic properties, have been formed via particle-mediated assembly.[2−4] Many researchers have studied the coalescence mechanisms of nanoparticles by *in situ* measurements and molecular dynamics (MD) simulations, which can potentially aid the management of the coalescence process during the synthesis for fine control of nanoparticle structures.[5−10] The coalescence process proceeds through the following steps: approach, contact, merging, and structural relaxation of nanoparticle pairs.[11] A jump-to-contact process has been observed where nanoparticle pairs quickly approach and stick together in a short interparticle distance, just before the contact.[12,13] Likewise, the degree of misalignment of a nanoparticle pair determines whether or not the coalesced nanoparticles contain a grain boundary.[14] When the nanoparticle pair exhibits a small angular misalignment, coalescence occurs through the orientated attachment, aligning the crystal planes of the pair, followed by the particle attachment, and the resulting particle tends to exhibit single crystallinity.[13]

Surface-passivating ligands are crucial factors in the synthesis of colloidal nanoparticles and are involved in the nanoparticle interactions and coalescence process.[15−18] The strength of the electrostatic and steric repulsive forces of the interacting nanoparticles is controlled by the charge and number densities of ligands placed between the nanoparticles.[19] Furthermore, the number density of the ligands adsorbed on different crystal facets is not uniform because the adsorption energy is facet dependent. These different ligand densities can potentially guide the occurrence of the coalescence along a specific direction where the facing surfaces are less hindered by the surface ligands.[13] Afterward, the morphology of the coalesced particles is determined by the facet-dependent stabilization of the surface ligands.[15−17] Thus, specific features in the kinetic

Received: August 31, 2020
Revised: November 8, 2020

ACS Publications © XXXX American Chemical Society

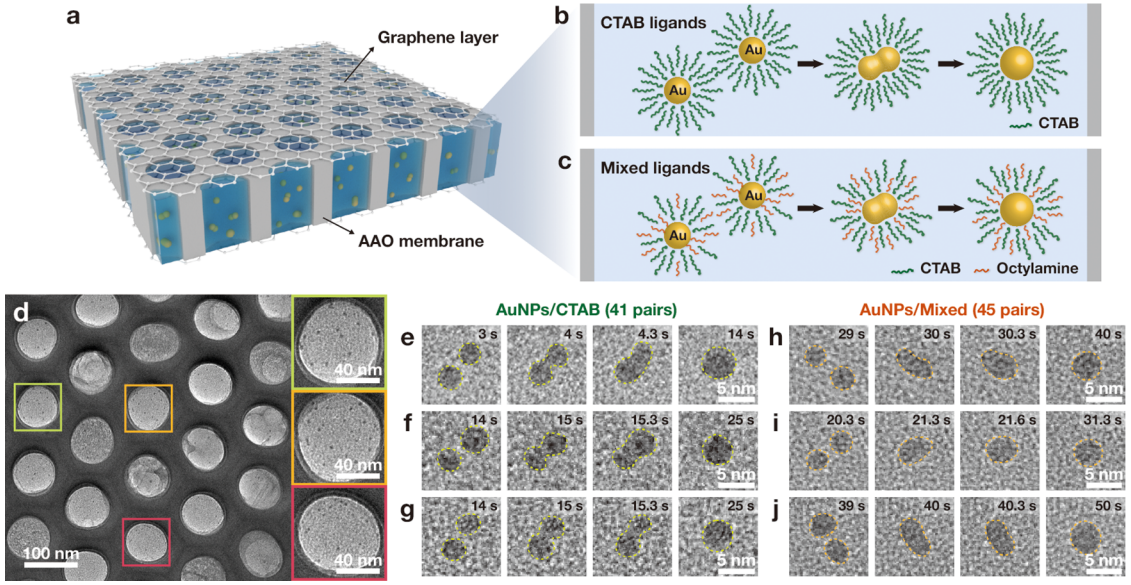

Figure 1. Schematics of (a) the multichamber graphene liquid cell and (b, c) the magnified views of the individual chambers in gold nanoparticle coalescence processes in different ligand environments, each of which contains pure CTAB (b; AuNPs/CTAB) or a mixture of CTAB and octylamine (c; AuNPs/Mixed). (d) TEM image of the regularly arranged multichambers containing colloidal gold nanoparticles. The images on the right column are the magnified views of the three representative chambers, with black dots inside the AAO hole indicating the nanoparticles. (e–j) Time series of the TEM images exhibiting the overall coalescence process in the (e–g) AuNPs/CTAB and (h–j) AuNPs/Mixed systems.

process of coalescence (from the approach, through merging, to structural relaxation) occurring in a real synthesis could differ, depending on the type, density, and molecular structure of the ligands utilized in the synthesis. More importantly, ligands as a mixture of two or more types, which are generally employed for the precise control of colloidal synthesis, endow additional complexity to the coalescence pathway.

In situ liquid-phase transmission electron microscopy (TEM) is an appropriate method that allows direct observations for understanding the detailed kinetic pathways of nanoparticle formation including coalescence.[20−28] However, it requires an additional capability to acquire numerous *in situ* trajectories under a controlled chemical condition in order to quantitatively distinguish the effects of different types of ligand systems on the coalescence kinetics. There have been recent technical developments of chamber-type liquid cell with defined dimensions for multiple liquid-phase TEM observations.[29−32] Here, employing quantitative liquid-phase TEM observation with a multichamber graphene liquid cell, we study the ligand-dependent coalescence behaviors of gold nanoparticles. The analyses of the numerous coalescence trajectories of the nanoparticles in the unicomponent and mixed-ligand systems, combined with MD simulations of ligand adsorption on the gold surfaces, elucidate that coalescence kinetics is ligand dependent and the increased mobility in the heterogeneous ligands results in a rapid approach of the nanoparticle pairs and reshaping after merging.

A multichamber graphene liquid cell is fabricated by sandwiching a nanoporous anodic aluminum oxide (AAO) membrane in graphene layers, whereby the loaded liquid sample is encapsulated between the graphene layers in each chamber, as illustrated in Figure 1a (Supporting Information).[33] The dimensions of the chamber are 70-80 nm (diameter) and 50-60 nm (depth). The average thickness of the 22 independent chambers encapsulating liquid samples is 39.8 ± 11.5 nm in a 60 nm thick AAO membrane (Figure S1). It is large enough to observe the nanoparticle growth that incorporates coalescence events whose critical steps typically occur in the sub 5 nm size range.[13,14,34] Because the multichambers are separated by the AAO matrix, the *in situ* TEM observation of one chamber does not induce a chemical perturbation in the other chambers. Additionally, the regular arrangement of the multichambers, at an interpore distance of 125 nm, allows the collection of the independent and cumulative *in situ* data by moving an area of the observation from one chamber to another. In this work, two types of aqueous gold precursor solutions, each of which contains pure hexadecyltrimethylammonium bromide (CTAB) or a mixture of CTAB and octylamine (3:1 molar ratio), are prepared as a different ligand system (Supporting Information). Each solution is observed by liquid-phase TEM to quantitatively compare the coalescence dynamics of gold nanoparticles in different ligand environments. CTAB is known to spontaneously form a bilayer coating on gold surfaces; thus, generated nanoparticles in the liquid cells are presumably capped with the CTAB ligands and mixed ligands (including CTAB and octylamine), respectively, and denoted as AuNPs/CTAB and AuNPs/Mixed (Figures 1b and 1c).[35−38] Low-magnification TEM imaging confirms that the multichambers are successfully formed and contain the liquid samples with gold nanoparticles (Figure 1d). The nanoparticles in the two different ligand systems dispersed in the multichambers are observed by *in situ* TEM, as shown in the two representative TEM movies (Movies S1 and S2). Generally, the gold nanoparticles grow from small to large sizes, following two major mechanistic pathways of monomer attachment and coalescence, as previously reported.[39] By performing repeated *in situ* TEM observations on the multichamber, 41 and 45 pairs of AuNPs/CTAB and AuNPs/Mixed, undergoing coalescence, are tracked for the quantitative comparison of the coalescence process under different capping ligand conditions (Movies S3 and S4). In all the observations, consistent beam parameters are employed (acceleration voltage of 200 kV; electron dose rate of 4000−8000 e^{-} $Å^{-2}$ s^{-1}). It is noteworthy that low-dose

https://dx.doi.org/10.1021/acs.nanolett.0c03517
Nano Lett. XXXX, XXX, XXX−XXX

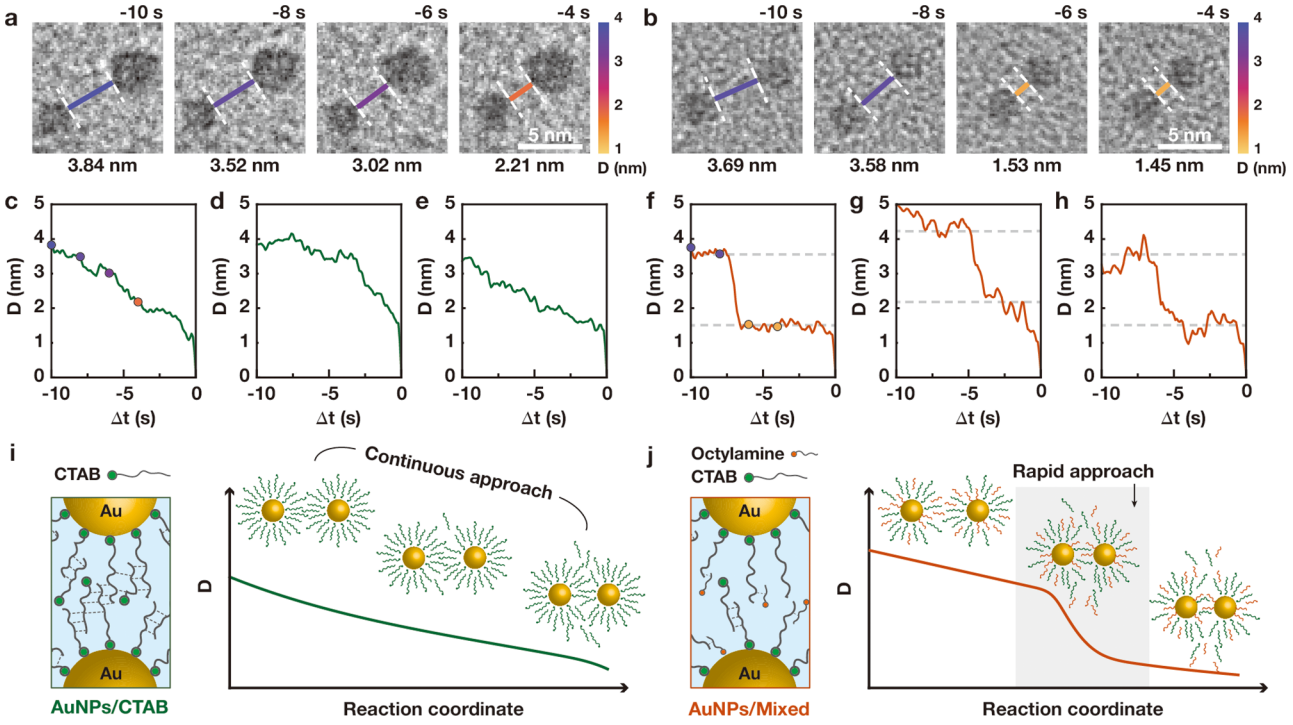

Figure 2. Time series of the TEM images exhibiting the approach behaviors of the gold nanoparticles in the (a) AuNPs/CTAB and (b) AuNPs/Mixed systems. For the upper values: time, $\Delta t = t - t_0$ with respect to t_0, at the instance of contact. For the lower values: D marked with a color stick. (c–e) The gap trajectories of the pairs in AuNPs/CTAB and (f–h) those of the pairs in AuNPs/Mixed before the surface contact of the nanoparticles. The color dots in (c) and (f) correspond to$D$ in (a) and (b), respectively. The illustration of the ligand interdigitation and approach behaviors of a pair in the (i) AuNPs/CTAB and (j) AuNPs/Mixed systems, respectively.

imaging of the identical samples (~50 to ~300 e^{-} $Å^{-2}$ s^{-1}) does not induce coalescence of AuNPs but induces their dissolution (Figure S2, see details in Supporting Information), consistent with the previous work.[40] The three representative coalescence trajectories of AuNPs/CTAB and AuNPs/Mixed are shown in Figures 1e–g and 1h–j, respectively. Each trajectory indicates that two gold nanoparticles approach each other to contact, after which they merge into a single nanoparticle followed by the structural relaxation process.

Next, we investigate the approach dynamics of the nanoparticle pairs, before their surfaces contact at t_0, by measuring the distance between their surfaces, gap (D), from the time series of the TEM images (Figures 2a–h and S3–S8; see details in the Supporting Information). In the AuNPs/CTAB system, D between the two nanoparticles gradually decreases as shown in the time series of the TEM images and their corresponding gap trajectory (Figures 2a and 2c). This behavior is universal in all tracked pairs of AuNPs/CTAB. Their gap trajectories (Figures 2c–e, S3, and S5) indicate that the nanoparticles capped with the CTAB ligands continuously approach each other, followed by the jump-to-contact where D is ~1 nm. Contrarily, the paring approach behavior in the AuNPs/Mixed system is different from that in the AuNPs/CTAB system. A representative time series of the TEM images and the corresponding gap trajectory of an AuNPs/Mixed pair demonstrate a rapid decrease in D, from ~3.5 nm (blue bar) to ~1.5 nm (yellow bar) (Figures 2b and 2f). This rapid pair approach is mostly observed in the AuNPs/Mixed system, which exhibits a noticeably sharp decrease in D in 22% of the 45 tracked pairs (Figures S4 and S6). The TEM images and their corresponding gap trajectories (Figures 2f–h, S4, and S7) indicate that the rapid decrease in D occurs in the distance ranges, from 3–6 to 1–2 nm. This range is presumably where the ligand shells, placed between the two interacting nanoparticles, are disassembled and pushed away by the approaching nanoparticle cores (Figure S9) since the length of one fully stretched CTAB molecule is ~2.2 nm and the CTAB molecules form interdigitated ligand shell, which is ~3.2 nm thick, as the surfactants of the colloidal nanoparticles.[41,42] When D becomes ~1 nm, the jump-to-contact occurs in all the AuNPs/Mixed pairs (Figure S5) like in the AuNPs/CTAB ones. The schematics of different ligand shell interdigitations and pair approach behaviors in the AuNPs/CTAB and AuNPs/Mixed systems are illustrated in Figures 2i and 2j. It is known that the CTAB molecules form an ordered bilayer structure with the partial interdigitation of long alkylchains in the ligand shell of a gold nanoparticle.[41,43] Thus, our liquid-phase TEM observations indicate that the incorporation of octylamine with a shorter alkylchain length than that of CTAB possibly modifies the ligand interdigitation and configuration of the ligand shell, which can result in differences in the approach behaviors of the nanoparticle pairs.

We perform MD simulations to understand the interdigitation characteristics and configurations of the ligand shell, constructed on the gold surfaces, according to the degree of mixing octylamine within the CTAB ligands. The simulations for four different ligand systems (0%, 25%, 33%, and 50% mixing ratios of octylamine to CTAB, denoted as C100, C75O25, C67O33, and C50O50, respectively) are performed on the gold (111), (110), and (100) surfaces (see details in the Supporting Information). The equilibrated configurations of the ligand shells of these systems are shown in Figure 3a. The configuration and thickness of the ligand shell in the pure CTAB system (C100) are consistent with previously reported

https://dx.doi.org/10.1021/acs.nanolett.0c03517
Nano Lett. XXXX, XXX, XXX−XXX

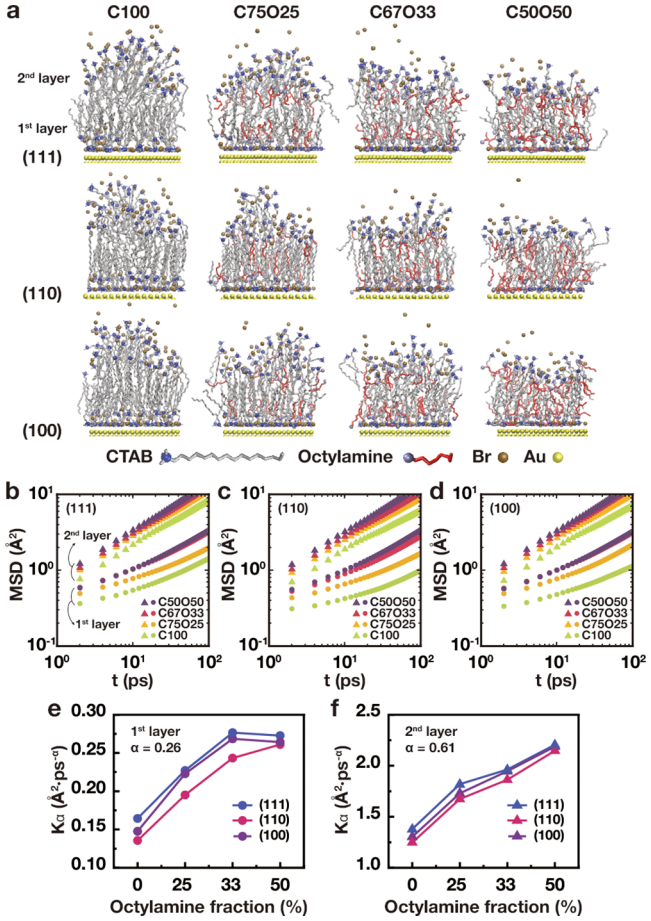

Figure 3. (a) MD simulations of the ligand shell configurations on the gold (111), (110), and (100) surfaces with different composition ratios of CTAB and octylamine. (b–d) Ensemble-averaged MSD for the ligands in the ligand shell on the gold (b) (111), (c) (110), and (d) (100) surfaces, calculated for all the systems in (a). Four plots with triangles and another four plots with circles in each graph correspond to the second and first layers of the ligand shell, respectively. The sub-diffusion coefficients, K_α, of the ligands in (e) the first and (f) second layers according to octylamine fraction.

results.[44] The ligand bilayer structure is formed on the gold surfaces in all systems, although their molecular arrangements are different. The thickness of the mixed ligand shell decreases slightly and the degree of the ligand disorder in the bilayer structure increases as the mixing ratio of octylamine increases (Figures S10 and 3a). Furthermore, we divide the ligands within the bilayered ligand shell into two groups, based on the direction of the ligand headgroup, i.e., those with the headgroup toward the gold surface and the others facing outward are categorized as the first and second layers, respectively. The ensemble-averaged mean square displacement (MSD) of the ligands in the first and second layers (Figures 3b–d), calculated from the simulations, affords the information on the diffusion behavior and mobility of the ligands. The ligands in all four systems exhibit sub-diffusive behaviors with diffusion exponents (α) of 0.26 and 0.61 for the first and second layers, which are less than the value of normal diffusion by 1.[45] This sub-diffusive motion of the ligands is presumably due to the confinement effect of the ligands by their interdigitation in the ligand shell.[45,46] Moreover, the ensemble-averaged MSD plots indicate that the ligands in the outer second layer are more mobile than those in the first layer, located near the gold surface, in all the (111), (110), and (100) surfaces (Figures 3b–d and S11). We calculate the sub-diffusion coefficients (K_α) from the ensemble-averaged MSD plots (Figures 3b–d) and present them in Figures 3e and 3f.[45] For all the surfaces, K_α in both the first and second layers increases as the octylamine fraction in the ligand shell increases (Figures 3e and 3f), indicating that the presence of octylamine increases the overall ligand mobility inside the shell (Figure S11). The interdigitation enthalpy between the alkylchains of CTAB is large enough to stabilize the CTAB bilayer structure.[47] However, by mixing octylamine, which possesses a shorter alkyl chain than CTAB, the interdigitation enthalpy can be lowered because the degree of alignment between the alkyl chains of the ligands is reduced.[48,49] Therefore, the MD simulation results suggest that the heterogeneous ligand system enables the freer movement of the constituent ligand molecules between the two interacting nanoparticles, thus resulting in rapid pair approach in the AuNPs/Mixed system, as observed in liquid-phase TEM.

We also track the neck formation and structural relaxation processes of the merged nanoparticles that occur after the surface contact (Supporting Information). The representative time series of the TEM images display the shape evolution of the coalesced nanoparticles in the AuNPs/CTAB and AuNPs/Mixed systems (Figures 4a and 4b). In both systems, a neck that connects the two nanoparticles is transiently formed in the gap just after the surface contact, at t_0, and the merged nanoparticles are gradually reconstructed into spherical shapes mainly by surface diffusion (Figures 1e–j, 4a, 4b, and S12). However, the rates of such shape evolution processes are noticeably different in the two systems. In the AuNPs/CTAB system (Figure 4a), the concave neck of the merged nanoparticle is visible until 2.4 s while the neck recovery proceeds quickly for ~1.2 s in the AuNPs/Mixed system (Figure 4b). The initial bridge length (s) of all the nanoparticle pairs is measured by subtracting the sum of the diameters of two nanoparticles, one frame before the contact (at $t = t_0 - 0.1$ s), from the end-to-end length along the long axis of the merged nanoparticles at the contact (at t_0). The positive and negative values of s indicate that merged nanoparticles exhibit dumbbell shapes with a protruding bridge and a snowman shapes with an overlapped volume of two nanoparticles, respectively (Figure 4c). Most of the merged nanoparticles in the AuNPs/CTAB system (green) exhibit the dumbbell shapes with an average length of ~0.5 nm for the protruding bridge. Conversely, both shapes appear in the AuNPs/Mixed system (orange) and 47% of the merged nanoparticles are snowman-shaped, possibly because of the rapid coalescing process of the pair. We further quantify the structural relaxation process of the merged nanoparticles by monitoring the evolution of their circularity (C) with time. As indicated in the exemplary pairs in Figures 4a and 4b, C is estimated from the 2D-projected images of the merged nanoparticles (Supporting Information), which asymptotically approaches 1 (implying a perfect circle) in both cases. However, the evolution speed of C is clearly different in the two ligand systems. In the AuNPs/CTAB system (Figure 4d), the C evolution pathways are widely distributed and require a prolonged time for C to approach 1. In the AuNPs/Mixed system (Figure 4e), >90% of the merged nanoparticles are rapidly reconstructed to a spherical shape within 5 s. We also calculate the rate constant of the relaxation processes (k), based on the fitting model where the difference between the measured C (Figures 4d and 4e) and 1 decays

https://dx.doi.org/10.1021/acs.nanolett.0c03517
Nano Lett. XXXX, XXX, XXX−XXX

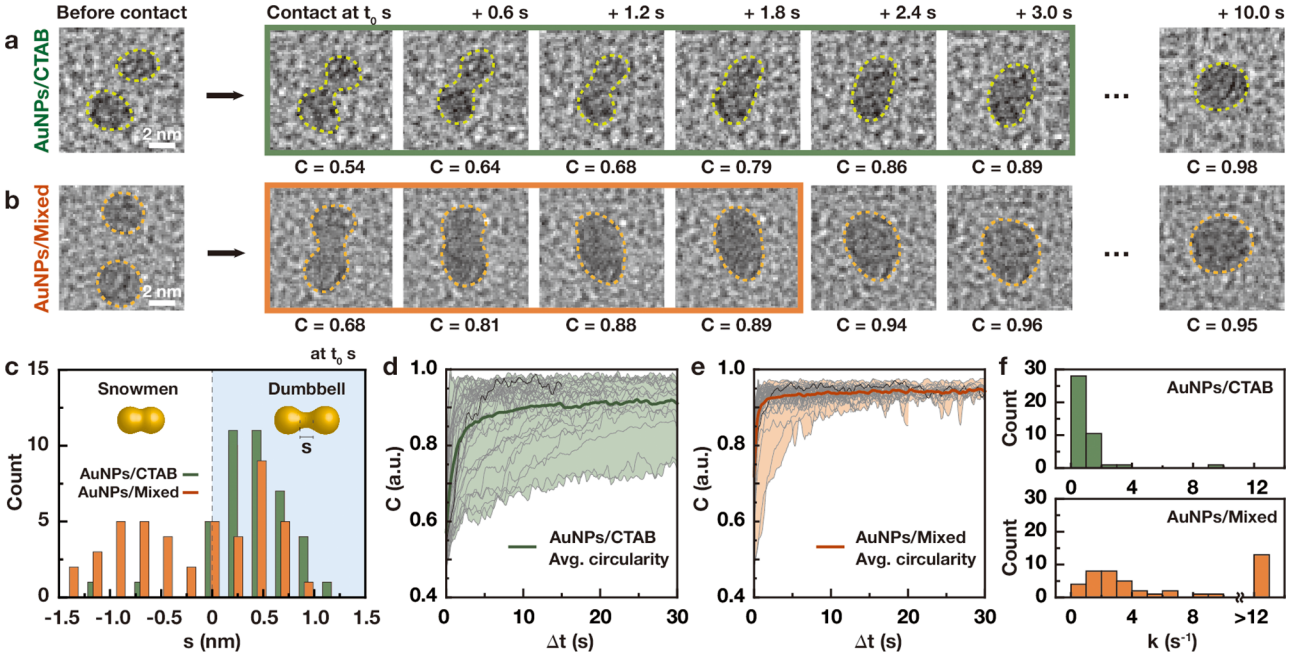

Figure 4. Time series of the TEM images exhibiting the neck formation and structural relaxation of the merged gold nanoparticles in the (a) AuNPs/CTAB and (b) AuNPs/Mixed systems. *C* is a circularity of merged nanoparticles. The bold-colored boxes indicate the times required to develop an equivalent *C* of 0.89 in the two systems. (c) Initial bridge length, *s*, just after the contact, at t_0, for the merged nanoparticles in the AuNPs/CTAB (green) and AuNPs/Mixed (orange) systems. The insets exhibit different shapes of the merged nanoparticles, according to the signs of *s*. Tracked circularity for the merged (d) 41 nanoparticles in AuNPs/CTAB and (e) 45 pairs of AuNPs/Mixed. The colored solid thick lines represent the mean value of *C* over time, and the black solid lines of (d) and (e) correspond to the circularity plots of the pairs in (a) and (b), respectively. (f) Exponential fitting parameter, *k*, of the merged nanoparticles in the AuNPs/CTAB (green) and AuNPs/Mixed (orange) systems, indicating the rate constant of the relaxation processes of the merged nanoparticles.

exponentially, $1 - C(\Delta t) = A \times e^{-k\Delta t}$. The histogram of *k* in the two systems (Figure 4f) demonstrates that the *k* values of most of the pairs in AuNPs/CTAB are less than 2 s^{-1}, while those of more than 70% of the pairs of AuNPs/Mixed are greater than 2 s^{-1} and those of ~30% are greater than 12 s^{-1}. The ligand structure and dynamics, modified by the heterogeneous mixing, are presumably attributed to the frequent observation of the snowman shapes after the contact and the fast evolution of *C* in the AuNPs/Mixed system. Enhanced ligand mobility, obtained by mixing octylamine in the CTAB ligands, is confirmed by our MD simulations. The enhanced mobility facilitates ligand detachment in the gap region at the instance of contact, thus inducing the fast merging dynamics. Additionally, the mobile surface ligands promote their rearrangement, which accompanies the surface-atom diffusion, to develop an isotropic morphology after the coalescence.

Summarily, we confirm that the coalescence behaviors of nanoparticles are highly dependent on their surface ligand structures by quantitative liquid-phase TEM, via employing multichamber graphene liquid cells, and MD simulations. We investigate the step-by-step processes of the nanoparticle coalescence that includes the approach, merging, and structural relaxation stages. Our results confirm that the enhanced mobility of the ligand system, obtained by mixing a short alkyl chain ligand, octylamine, in the well-structured CTAB bilayer, induces the rapid approach of the nanoparticle pair and the fast structural reorganization of the coalesced nanoparticles.

■ ASSOCIATED CONTENT

Supporting Information

The Supporting Information is available free of charge at https://pubs.acs.org/doi/10.1021/acs.nanolett.0c03517.

Experimental details, MD simulations details, and supporting figures (PDF)

(Movie S1) *In situ* liquid-phase TEM movie of the gold nanoparticles capped with the CTAB ligands inside a multichamber (MP4); (Movie S2) *in situ* liquid-phase TEM movie of the gold nanoparticles capped with the CTAB ligands inside a multichamber (MP4); (Movie S3) *in situ* liquid-phase TEM movie of the coalescence of 41 pairs in the AuNPs/CTAB system (MP4); and (Movie S4) *in situ* liquid-phase TEM movie of the coalescence of 45 pairs in the AuNPs/mixed system (MP4) (ZIP)

■ AUTHOR INFORMATION

Corresponding Authors

Jungwon Park − *School of Chemical and Biological Engineering, and Institute of Chemical Processes, Seoul National University, Seoul 08826, Republic of Korea; Center for Nanoparticle Research, Institute of Basic Science (IBS), Seoul 08826, Republic of Korea;* orcid.org/0000-0003-2927-4331; Email: jungwonpark@snu.ac.kr

Won Chul Lee − *Department of Mechanical Engineering, Major in Materials, Devices, and Equipment, Hanyang University, Ansan, Gyeonggi 15588, Republic of Korea;* orcid.org/0000-0001-8479-0836; Email: wonchullee@hanyang.ac.kr

https://dx.doi.org/10.1021/acs.nanolett.0c03517
Nano Lett. XXXX, XXX, XXX−XXX

Won Bo Lee − *School of Chemical and Biological Engineering, and Institute of Chemical Processes, Seoul National University, Seoul 08826, Republic of Korea;* orcid.org/0000-0001-7801-083X; Email: wblee@snu.ac.kr

Authors

Yuna Bae − *School of Chemical and Biological Engineering, and Institute of Chemical Processes, Seoul National University, Seoul 08826, Republic of Korea; Center for Nanoparticle Research, Institute of Basic Science (IBS), Seoul 08826, Republic of Korea*

Kitaek Lim − *Department of Mechanical Engineering, Major in Materials, Devices, and Equipment, Hanyang University, Ansan, Gyeonggi 15588, Republic of Korea*

Seulwoo Kim − *School of Chemical and Biological Engineering, and Institute of Chemical Processes, Seoul National University, Seoul 08826, Republic of Korea*

Dohun Kang − *School of Chemical and Biological Engineering, and Institute of Chemical Processes, Seoul National University, Seoul 08826, Republic of Korea; Center for Nanoparticle Research, Institute of Basic Science (IBS), Seoul 08826, Republic of Korea*

Byung Hyo Kim − *School of Chemical and Biological Engineering, and Institute of Chemical Processes, Seoul National University, Seoul 08826, Republic of Korea; Center for Nanoparticle Research, Institute of Basic Science (IBS), Seoul 08826, Republic of Korea; Department of Organic Materials and Fiber Engineering, Soongsil University, Seoul 06978, Republic of Korea;* orcid.org/0000-0002-4098-0053

Joodeok Kim − *School of Chemical and Biological Engineering, and Institute of Chemical Processes, Seoul National University, Seoul 08826, Republic of Korea; Center for Nanoparticle Research, Institute of Basic Science (IBS), Seoul 08826, Republic of Korea*

Sungsu Kang − *School of Chemical and Biological Engineering, and Institute of Chemical Processes, Seoul National University, Seoul 08826, Republic of Korea; Center for Nanoparticle Research, Institute of Basic Science (IBS), Seoul 08826, Republic of Korea*

Sungho Jeon − *Department of Mechanical Engineering, Major in Materials, Devices, and Equipment, Hanyang University, Ansan, Gyeonggi 15588, Republic of Korea*

JunBeom Cho − *School of Chemical and Biological Engineering, and Institute of Chemical Processes, Seoul National University, Seoul 08826, Republic of Korea*

Complete contact information is available at: https://pubs.acs.org/10.1021/acs.nanolett.0c03517

Author Contributions

The manuscript was written through contributions of all authors. All authors have given approval to the final version of the manuscript.

Notes

The authors declare no competing financial interest.

■ ACKNOWLEDGMENTS

This article is dedicated to the people fighting against the Coronavirus disease (COVID-19) pandemic. This work was supported by the Institute for Basic Science (IBS-R006-D1). Y.B., D.K., B.H.K., J.K., S.K., and J.P. acknowledge the financial support from the NRF grant funded by the Korean government (MSIT) (NRF-2017R1A5A1015365 and NRF-2019M3E6A1064877). B.H.K. and J.P. acknowledge the support from the Samsung Science and Technology Foundation under project number SSTF-BA1802-08 for method development, fabrication, and characterization. K.L., S.J., and W.C.L. acknowledge the support from the National Research Foundation of Korea (NRF) funded by the Ministry of Education (2019R1F1A1059099 and 2020R1F1A1065856) and the support from the research fund of Hanyang University (HY-2018-N). S.K., J.-B.C., and W.B.L. acknowledge the support from the Creative Material Discovery Project through the NRF grant funded by the Korean government (MSIT) (2018M3D1A1058633).

■ NOMENCLATURE

MD, molecular dynamics
TEM, transmission electron microscopy
AAO, anodic aluminum oxide
CTAB, hexadecyltrimethylammonium bromide
AuNPs, gold nanoparticles
MSD, mean square displacement

■ REFERENCES

(1) Kumar, M.; Deka, S. Multiply Twinned Agni Alloy Nanoparticles as Highly Active Catalyst for Multiple Reduction and Degradation Reactions. *ACS Appl. Mater. Interfaces* **2014**, *6*, 16071−16081.

(2) Lim, B.; Xia, Y. Metal Nanocrystals with Highly Branched Morphologies. *Angew. Chem., Int. Ed.* **2011**, *50*, 76−85.

(3) Wang, Y.; Camargo, P. H.; Skrabalak, S. E.; Gu, H.; Xia, Y. A facile, water-based synthesis of highly branched nanostructures of silver. *Langmuir* **2008**, *24*, 12042−12046.

(4) Lim, B.; Jiang, M.; Yu, T.; Camargo, P. H.; Xia, Y. Nucleation and growth mechanisms for Pd-Pt bimetallic nanodendrites and their electrocatalytic properties. *Nano Res.* **2010**, *3*, 69−80.

(5) Ingham, B.; Lim, T. H.; Dotzler, C. J.; Henning, A.; Toney, M. F.; Tilley, R. D. How nanoparticles coalesce: an in situ study of Au nanoparticle aggregation and grain growth. *Chem. Mater.* **2011**, *23*, 3312−3317.

(6) Li, J.; Chen, J.; Wang, H.; Chen, N.; Wang, Z.; Guo, L.; Deepak, F. L. In Situ Atomic-Scale Study of Particle-Mediated Nucleation and Growth in Amorphous Bismuth to Nanocrystal Phase Transformation. *Adv. Sci.* **2018**, *5*, 1700992.

(7) Grammatikopoulos, P.; Sowwan, M.; Kioseoglou, J. Computational modeling of nanoparticle coalescence. *Adv. Theor. Simul.* **2019**, *2*, 1900013.

(8) Grammatikopoulos, P.; Cassidy, C.; Singh, V.; Sowwan, M. Coalescence-induced crystallisation wave in Pd nanoparticles. *Sci. Rep.* **2014**, *4*, 5779.

(9) Wang, J.; Chen, S.; Cui, K.; Li, D.; Chen, D. Approach and coalescence of gold nanoparticles driven by surface thermodynamic fluctuations and atomic interaction forces. *ACS Nano* **2016**, *10*, 2893−2902.

(10) Liao, H. G.; Cui, L.; Whitelam, S.; Zheng, H. Real-time imaging of Pt_3Fe nanorod growth in solution. *Science* **2012**, *336*, 1011−1014.

(11) Jose-Yacaman, M.; Gutierrez-Wing, C.; Miki, M.; Yang, D. Q.; Piyakis, K. N.; Sacher, E. Surface diffusion and coalescence of mobile metal nanoparticles. *J. Phys. Chem. B* **2005**, *109*, 9703−9711.

(12) Li, D.; Nielsen, M. H.; Lee, J. R.; Frandsen, C.; Banfield, J. F.; De Yoreo, J. J. Direction-specific interactions control crystal growth by oriented attachment. *Science* **2012**, *336*, 1014−1018.

(13) Zhu, C.; Liang, S.; Song, E.; Zhou, Y.; Wang, W.; Shan, F.; Shi, Y.; Hao, C.; Yin, K.; Zhang, T.; Liu, J.; Zheng, H.; Sun, L. In-situ liquid cell transmission electron microscopy investigation on oriented attachment of gold nanoparticles. *Nat. Commun.* **2018**, *9*, 1−7.

(14) Aabdin, Z.; Lu, J.; Zhu, X.; Anand, U.; Loh, N. D.; Su, H.; Mirsaidov, U. Bonding pathways of gold nanocrystals in solution. *Nano Lett.* **2014**, *14*, 6639−6643.
(15) Ortiz, N.; Skrabalak, S. E. On the dual roles of ligands in the synthesis of colloidal metal nanostructures. *Langmuir* **2014**, *30*, 6649−6659.
(16) Heuer-Jungemann, A.; Feliu, N.; Bakaimi, I.; Hamaly, M.; Alkilany, A.; Chakraborty, I.; Masood, A.; Casula, M. F.; Kostopoulou, A.; Oh, E.; Susumu, K.; Stewart, M. H.; Medintz, I. L.; Stratakis, E.; Parak, W. J.; Kanaras, A. G. The role of ligands in the chemical synthesis and applications of inorganic nanoparticles. *Chem. Rev.* **2019**, *119*, 4819−4880.
(17) Wang, W.; Banerjee, S.; Jia, S.; Steigerwald, M. L.; Herman, I. P. Ligand control of growth, morphology, and capping structure of colloidal CdSe nanorods. *Chem. Mater.* **2007**, *19*, 2573−2580.
(18) Guo, P.; Gao, Y. Coalescence of Au Nanoparticles without Ligand Detachment. *Phys. Rev. Lett.* **2020**, *124*, No. 066101.
(19) Si, K. J.; Chen, Y.; Shi, Q.; Cheng, W. Nanoparticle superlattices: the roles of soft ligands. *Adv. Sci.* **2018**, *5*, 1700179.
(20) Ross, F. M. *Liquid Cell Electron Microscopy*, 1st ed.; Cambridge University Press: Cambridge, 2016.
(21) Kim, B. H.; Yang, J.; Lee, D.; Choi, B. K.; Hyeon, T.; Park, J. Liquid-phase transmission electron microscopy for studying colloidal inorganic nanoparticles. *Adv. Mater.* **2018**, *30*, 1703316.
(22) De Yoreo, J. J.; Sommerdijk, N. A. Investigating materials formation with liquid-phase and cryogenic TEM. *Nat. Rev. Mater.* **2016**, *1*, 1−18.
(23) Ou, Z.; Wang, Z.; Luo, B.; Luijten, E.; Chen, Q. Kinetic pathways of crystallization at the nanoscale. *Nat. Mater.* **2020**, *19*, 450−455.
(24) Liao, H. G.; Zherebetskyy, D.; Xin, H.; Czarnik, C.; Ercius, P.; Elmlund, H.; Pan, M.; Wang, L. W.; Zheng, H. Facet development during platinum nanocube growth. *Science* **2014**, *345*, 916−919.
(25) Anand, U.; Lu, J.; Loh, D.; Aabdin, Z.; Mirsaidov, U. Hydration layer-mediated pairwise interaction of nanoparticles. *Nano Lett.* **2016**, *16*, 786−790.
(26) Jin, B.; Sushko, M. L.; Liu, Z.; Jin, C.; Tang, R. In situ liquid cell TEM reveals bridge-induced contact and fusion of Au nanocrystals in aqueous solution. *Nano Lett.* **2018**, *18*, 6551−6556.
(27) Zheng, H.; Smith, R. K.; Jun, Y. W.; Kisielowski, C.; Dahmen, U.; Alivisatos, A. P. Observation of single colloidal platinum nanocrystal growth trajectories. *Science* **2009**, *324*, 1309−1312.
(28) Yuk, J. M.; Park, J.; Ercius, P.; Kim, K.; Hellebusch, D. J.; Crommie, M. F.; Lee, J. Y.; Zettl, A.; Alivisatos, A. P. High-resolution EM of colloidal nanocrystal growth using graphene liquid cells. *Science* **2012**, *336*, 61−64.
(29) Rasool, H.; Dunn, G.; Fathalizadeh, A.; Zettl, A. Graphene-sealed Si/SiN cavities for high-resolution in situ electron microscopy of nano-confined solutions. *Phys. Status Solidi B* **2016**, *253* (12), 2351−2354.
(30) Wadell, C.; Inagaki, S.; Nakamura, T.; Shi, J.; Nakamura, Y.; Sannomiya, T. Nanocuvette: a functional ultrathin liquid container for transmission electron microscopy. *ACS Nano* **2017**, *11*, 1264−1272.
(31) Kelly, D. J.; Zhou, M.; Clark, N.; Hamer, M. J.; Lewis, E. A.; Rakowski, A. M.; Haigh, S. J.; Gorbachev, R. V. Nanometer resolution elemental mapping in graphene-based TEM liquid cells. *Nano Lett.* **2018**, *18* (2), 1168−1174.
(32) Hutzler, A.; Schmutzler, T.; Jank, M. P.; Branscheid, R.; Unruh, T.; Spiecker, E.; Frey, L. Unravelling the Mechanisms of Gold−Silver Core−Shell Nanostructure Formation by in Situ TEM Using an Advanced Liquid Cell Design. *Nano Lett.* **2018**, *18* (11), 7222−7229.
(33) Lim, K.; Bae, Y.; Jeon, S.; Kim, K.; Kim, B. H.; Kim, J.; Kang, S.; Heo, T.; Park, J.; Lee, W. C. A Large Scale Array of Ordered Graphene Sandwiched Chambers for Quantitative Liquid Phase Transmission Electron Microscopy. *Adv. Mater.* **2020**, *32*, 2002889.
(34) Wuithschick, M.; Witte, S.; Kettemann, F.; Rademann, K.; Polte, J. Illustrating the formation of metal nanoparticles with a growth concept based on colloidal stability. *Phys. Chem. Chem. Phys.* **2015**, *17*, 19895−19900.
(35) Nikoobakht, B.; El-Sayed, M. A. Evidence for bilayer assembly of cationic surfactants on the surface of gold nanorods. *Langmuir* **2001**, *17*, 6368−6374.
(36) Sau, T. K.; Murphy, C. J. Self-assembly patterns formed upon solvent evaporation of aqueous cetyltrimethylammonium bromide-coated gold nanoparticles of various shapes. *Langmuir* **2005**, *21*, 2923−2929.
(37) Tian, Y.; Yu, B.; Li, X.; Li, K. Facile solvothermal synthesis of monodisperse Fe_3O_4 nanocrystals with precise size control of one nanometre as potential MRI contrast agents. *J. Mater. Chem.* **2011**, *21*, 2476−2481.
(38) Baruah, B.; Kiambuthi, M. Facile synthesis of silver and bimetallic silver−gold nanoparticles and their applications in surface-enhanced Raman scattering. *RSC Adv.* **2014**, *4*, 64860−64870.
(39) Lee, J.; Yang, J.; Kwon, S. G.; Hyeon, T. Nonclassical nucleation and growth of inorganic nanoparticles. *Nat. Rev. Mater.* **2016**, *1*, 1−16.
(40) Schneider, N. M.; Norton, M. M.; Mendel, B. J.; Grogan, J. M.; Ross, F. M.; Bau, H. H. Electron−water interactions and implications for liquid cell electron microscopy. *J. Phys. Chem. C* **2014**, *118*, 22373−22382.
(41) Gómez-Graña, S.; Hubert, F.; Testard, F.; Guerrero-Martínez, A.; Grillo, I.; Liz-Marzán, L. M.; Spalla, O. Surfactant (bi) layers on gold nanorods. *Langmuir* **2012**, *28*, 1453−1459.
(42) Venkataraman, N. V.; Vasudevan, S. Hydrocarbon chain conformation in an intercalated surfactant monolayer and bilayer. *Proc. - Indian Acad. Sci., Chem. Sci.* **2001**, *113*, 539−558.
(43) Orendorff, C. J.; Alam, T. M.; Sasaki, D. Y.; Bunker, B. C.; Voigt, J. A. Phospholipid− gold nanorod composites. *ACS Nano* **2009**, *3*, 971−983.
(44) Meena, S. K.; Sulpizi, M. Understanding the microscopic origin of gold nanoparticle anisotropic growth from molecular dynamics simulations. *Langmuir* **2013**, *29*, 14954−14961.
(45) Metzler, R.; Jeon, J. H.; Cherstvy, A. G.; Barkai, E. Anomalous diffusion models and their properties: non-stationarity, non-ergodicity, and ageing at the centenary of single particle tracking. *Phys. Chem. Chem. Phys.* **2014**, *16*, 24128−24164.
(46) Babayekhorasani, F.; Dunstan, D. E.; Krishnamoorti, R.; Conrad, J. C. Nanoparticle diffusion in crowded and confined media. *Soft Matter* **2016**, *12*, 8407−8416.
(47) Jalali, F.; Gerandaneh, A. Micellization of cetyltrimethylammonium bromide (CTAB) in mixed solvents and in the presence of potassium bromide. *J. Dispersion Sci. Technol.* **2011**, *32*, 659−666.
(48) Yang, Y.; Qin, H.; Peng, X. Intramolecular entropy and size-dependent solution properties of nanocrystal−ligands complexes. *Nano Lett.* **2016**, *16*, 2127−2132.
(49) Moulik, S. P.; Haque, M. E.; Jana, P. K.; Das, A. R. Micellar properties of cationic surfactants in pure and mixed states. *J. Phys. Chem.* **1996**, *100*, 701−708.

https://dx.doi.org/10.1021/acs.nanolett.0c03517
Nano Lett. XXXX, XXX, XXX−XXX